Effects of decalcification on the microstructure and surface area of cement and tricalcium silicate pastes

Jeffrey J. Thomas[a,*], Jeffrey J. Chen[b], Andrew J. Allen[c], Hamlin M. Jennings[a,b]

[a]*Department of Civil and Environmental Engineering, Northwestern University, Evanston, IL 60208, USA*
[b]*Department of Materials Science and Engineering, Northwestern University, Evanston, IL 60208, USA*
[c]*Materials Science and Engineering Laboratory, National Institute of Standards and Technology, Gaithersburg, MD 20899, USA*

Abstract

Thin coupons of white portland cement (WPC) and tricalcium silicate paste were decalcified by leaching in concentrated ammonium nitrate solutions, resulting in calcium-to-silicon molar ratios (C/S) ranging from 3.0 (control) down to 0.3. The microstructure and surface area were measured using both small-angle neutron scattering (SANS) and nitrogen gas sorption. The intensity in the SANS data regime corresponding to the volume fractal C-S-H gel phase increased significantly on leaching, and the total surface area per unit specimen volume measured by SANS doubled on leaching from C/S = 3.0 to near C/S = 1.0. The nitrogen BET surface area of the WPC pastes, expressed in the same units, increased on decalcification as well, although not as sharply. The primary cause of these changes is a transformation of the high-density "inner product" C-S-H gel, which normally has a low specific surface area as measured by SANS and nitrogen gas sorption, into a morphology with a high specific surface area. The volume fractal exponent corresponding to the C-S-H gel phase decreased with decalcification from 2.3 to 2.0, indicating that the equiaxed 5 nm C-S-H globule building blocks that form the volume fractal microstructure of normal, unleached cement paste are transformed by decalcification into sheetlike structures of increasing thickness.
© 2004 Elsevier Ltd. All rights reserved.

Keywords: Calcium silicate hydrate (C-S-H); Microstructure; Small-angle neutron scattering; Surface area; Degradation

1. Introduction

Decalcification of cement paste is closely associated with various types of concrete deterioration. Important examples include leaching by exposure to flowing fresh water or weak acids, which removes calcium from the paste altogether, and external sulfate attack, which reorganizes the cement paste in such a way that the calcium in portlandite $[Ca(OH)_2 = CH^1]$ and in C-S-H gel is transferred to gypsum and ettringite. The addition of mineral admixtures, such as silica fume and blast furnace slag, to cement paste causes a similar reorganization, with a lower Ca form of C-S-H gel forming at the expense of CH and the typical high-Ca form of C-S-H gel. In recent years, the kinetics of calcium leaching [1,2] and the

effects of decalcification on the mechanical properties of cement paste [3–6], the solubility of C-S-H phases [7], and the chemical structure of C-S-H [8–10] have been studied and modeled. What is missing at present is a full understanding of the effects of decalcification, or changes in the calcium-to-silicon ratio (C/S), on the morphology [11] and nanometer-level structure of C-S-H. This paper reports results of small-angle neutron scattering (SANS) and nitrogen gas sorption experiments on tricalcium silicate (C_3S) and white portland cement (WPC) pastes leached to different C/S.
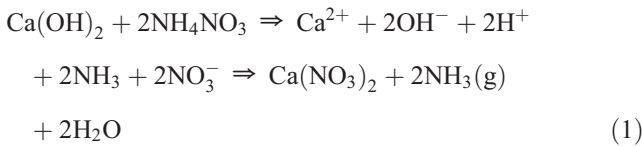
An experimental difficulty with leaching studies is the very long time required to leach in fresh water. Leaching cement pastes in concentrated solutions of NH_4NO_3 can reduce leaching times from weeks or months to hours. The increased rate of calcium dissolution in NH_4NO_3 can be attributed to a significant increase in the equilibrium calcium solubility. For example, Heukamp et al. [5] have estimated that the equilibrium calcium concentration of a solution saturated in CH increases from 0.022 mol/l in

---

* Corresponding author.
E-mail address: jthomas@northwestern.edu (J.J. Thomas).
[1] Cement chemistry notation: C = CaO, S = SiO_2, H = H_2O, A = Al_2O_3, F = Fe_2O_3.

pure water to approximately 2.9 mol/l in a 6-mol/l solution of NH_4NO_3. The dissolution of CH in the latter solution follows [5]:

$$Ca(OH)_2 + 2NH_4NO_3 \Rightarrow Ca^{2+} + 2OH^- + 2H^+$$
$$+ 2NH_3 + 2NO_3^- \Rightarrow Ca(NO_3)_2 + 2NH_3(g)$$
$$+ 2H_2O \qquad\qquad (1)$$

The removal of NH_3 from the solution as gas bubbles drives the reactions in Eq. (1) to the right, allowing large amounts of calcium to dissolve without approaching equilibrium. Previous work has established that the effects on the microstructure of leaching in NH_4NO_3 are similar to the effects of leaching in water or weakly acidic solutions [7,12]. The primary difference, other than the kinetics, is that NH_4NO_3 leaching preferentially removes calcium from the C-S-H even at very low C/S, whereas water leaching removes increasing amounts of silicon as the C/S falls below 1. The preservation of the Si structure allows very low C/S (near 0.1) to be reached while maintaining the integrity of the specimen.

In this study, thin (0.8 mm thick) coupons of paste were leached to various C/S. The use of thin specimens reduced the gradients in C/S across the specimen, and allowed the average C/S to be used to characterize the entire coupon. SANS was used to measure the specific surface area and the microstructure of saturated coupons, and nitrogen gas sorption was used to measure the surface area of dried companion specimens. Changes in the solubility [7] and chemical structure [7,10] as a function of C/S are reported elsewhere. Those results indicate that the leaching process of a cement or C_3S paste can be divided into three slightly overlapping regimes: (1) dissolution of CH, (2) removal of Ca−OH groups from the C-S-H gel (C/S = 1.7 to 1.2), and (3) removal of calcium associated with Si−O−Ca bonds in the interlayer spacings of C-S-H at C/S < 1.2. Step 3 is accompanied by a rapid increase in the degree of polymerization of the silicate chains.

2. Application of SANS to cement paste

Small-angle scattering with either neutrons (SANS) or X-rays (SAXS) has been used successfully to characterize the microstructure of cement and C_3S pastes [13–17]. In both cases, an intense beam is passed through a thin specimen, and a small component is scattered out of the incident beam direction by interactions with microstructural features within the bulk of the material. The volume of material probed (approximately 25 mm^3 in the present study) is large enough to represent a statistical average of the cement paste microstructure where the relevant scale lengths range from 1 nm to 10 μm. Scattering techniques are ideal for characterizing cement paste because specimens can be studied in their

natural saturated state, thus avoiding complications associated with drying the C-S-H gel [18]. In addition, small-angle scattering is particularly appropriate for this investigation because it is most effective in probing features in the 1- to 100-nm size range that defines critical aspects of the C-S-H gel structure. In cementitious systems, the scattering is dominated by the interface between the solid C-S-H and the smallest gel pores. However, comparisons of the rate of the SANS surface area development with the rate of heat evolution [16] and with the rate of bound water development [19] show that that while SANS and SAXS are sensitive to the open nanoscale gel/pore structure associated with the low-density "outer-product" C-S-H that forms in the water-filled capillary spaces of the paste, they (like nitrogen gas sorption) have little sensitivity to the dense, closed C-S-H structure that forms within the original boundaries of the anhydrous cement particles. A recent model [20] accounts for much of the quantitative data, including surface area values obtained from different techniques, by proposing different structures for high- and low-density C-S-H. Clearly, this distinction is important if the leaching process transforms the high-density morphology of C-S-H into low-density product with a large specific surface area.

Small-angle scattering studies generally report data as a function of the scattering vector, Q:

$$Q = \frac{4\pi}{\lambda} \sin\left(\frac{\theta}{2}\right) \qquad\qquad (2)$$

where θ is the angle of scatter and λ is the neutron wavelength. The Q-independent background scattering is subtracted from the data, and the data are absolutely calibrated using a standard scatterer. The resulting neutron scattering intensity, I, decreases strongly with increasing Q, and it is generally this loss of intensity that determines the experimental upper limit of Q. Note however, that many of the data reported here are plotted as $\log(IQ^4)$ versus $\log(Q)$, and the term IQ^4 actually increases with Q (plots of this form allow subtle features in the data to be more readily observed).

Fig. 1 shows the SANS scattering data [here plotted as $\log(I)$ versus $\log(Q)$] for an ordinary portland cement (OPC) paste measured at 7 h and at 44 h after mixing, illustrating the type of information that can be obtained from SANS. At small Q values, the largest features are probed, which for a young cement paste are the original cement clinker grains. The data at Q values below about 0.2 nm^{-1} can be modeled as a surface fractal regime, with the surface of the clinker grains becoming roughened by the formation of hydration product. Note the decrease in intensity at low Q with hydration time, as the clinker grains are consumed. At higher Q values, smaller features are probed, and the response is dominated by the low-density C-S-H gel. Thus, the intensity increases significantly between 7 and 44 h due to the early rapid hydration reaction. The scattering response
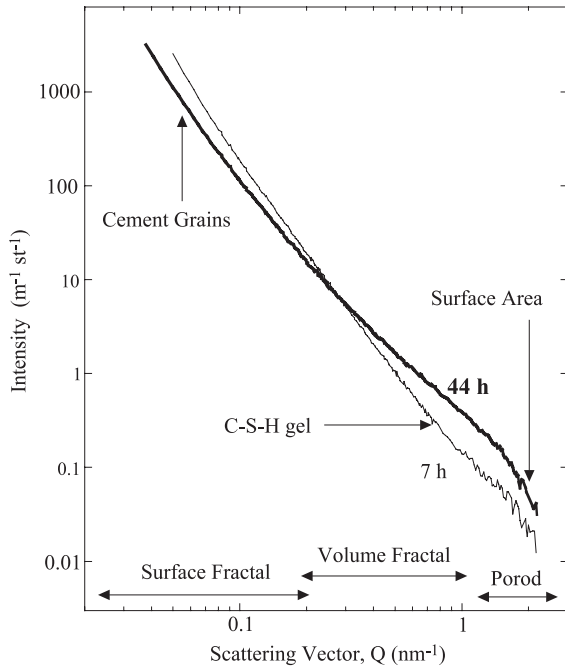
Fig. 1. SANS data for the same OPC paste after hydration for 7 h and 44 h. As the scattering vector (or angle) increases, scattering occurs from smaller features in the microstructure.

in the Q range of about $0.3-1.0$ nm^{-1} exhibits volume fractal behavior [13], such that $I \propto Q^{-x}$, where the scaling exponent, x, is close to 2.5. On a log–log plot of IQ^4 versus Q, this results in a linear region with positive slope $4 - x$. Previous analysis of the data in the volume fractal regime of cement paste has demonstrated that the scattering can be accounted for by a so-called diffusion-limited single-particle aggregate structure consisting of roughly equiaxed C-S-H gel particles about 5 nm in diameter [13]. The 5 nm building block size usually can also be inferred from a brief regime of associated Guinier scattering in the Q range $0.8-1.2$ nm^{-1}.

At high Q, the intensity of the scattering becomes proportional to the total internal surface area of the specimen; this is known as Porod scattering. For mature cement paste, the Porod region begins at about 1.4 nm^{-1} [16]. The surface area of hydrated cement paste arises almost entirely from the C-S-H gel, with only small additional contributions from other phases, such as CH. In a two-phase specimen, the total internal surface between the two phases can be determined from:

$$S_v = \frac{C_P}{2\pi |\Delta\rho^2|} \qquad (3)$$

where S_V is the surface area per unit volume, C_P is the Porod constant, and $|\Delta\rho^2|$ is the scattering contrast. The Porod constant is determined from the SANS data in the high scattering angle region of the scattering curve (after the background is subtracted). For data plotted in the form

shown in Fig. 2, the Porod constant is the y-axis value of the data at highest Q.

The scattering contrast is a parameter that measures the intrinsic strength of the neutron scattering interaction at the interface between two phases. For cement-based materials, the dominant scattering contrast is that between C-S-H gel and pore fluid, and the neutron scattering contrast can be written as:

$$|\Delta\rho|^2 = (\rho_{CSH} - \rho_{H2O})^2 \qquad (4)$$

where ρ_{CSH} and ρ_{H2O} are the neutron scattering length densities of C-S-H and of water. These are material parameters that can be calculated from the average chemical composition and density of the phase, using published tables [21]. This calculation is straightforward for well-defined phases, such as water and CH, but it presents a problem for the C-S-H gel due to its variable composition and poorly defined structure. A particular problem associated with the composition of C-S-H gel is that it is not clear how much water should be included in the solid phase for the purpose of calculating ρ_{CSH}.

Important information about the neutron scattering contrast for cement can be obtained experimentally by taking advantage of the large difference in neutron scattering length density between H_2O and D_2O (heavy water) [22,23]. When a hydrated cement paste is placed into D_2O, the D_2O exchanges fully with both the pore water and the water in the C-S-H gel, including structural water existing as OH$^-$ groups, and this greatly alters the scattering
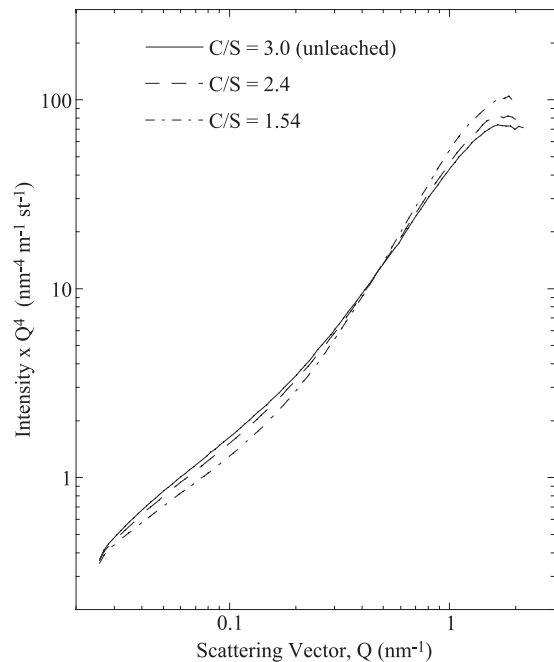

Fig. 2. SANS response of unleached and moderately leached 6-month-old WPC pastes. The decrease in scattering intensity at low Q can be attributed to the removal of calcium hydroxide.

contrast. When the change in the scattering contrast is measured as a function of D_2O content, the result for a two-phase system, such as C-S-H and water, is a parabola with a minimum value of zero contrast. The contrast is zero when the neutron scattering length density of the solid and liquid are equal (see Eq. (4)); this is termed the contrast matchpoint.

In a system with more than one solid phase that contributes to the high-Q scattering, the measured contrast variation curve will be the sum of the individual parabolas for the different solid/water systems, resulting in a single parabola that has a minimum value greater than zero. In (unleached) cement paste, the contrast variation parabola does not go completely to zero, due to small scattering contributions from fine CH crystals. The contribution from CH can be subtracted out, because the neutron scattering length density for CH is known, allowing the C-S-H parabola (and contrast matchpoint) to be determined.

Once the contrast matchpoint for C-S-H is known, the neutron scattering length density can be determined if any two of the three relevant physical parameters (C/S, H_2O/Si, and density) are known. The neutron scattering length density of the C-S-H gel in normal cement pastes has recently been established to be in the range $(2.55-2.90) \times 10^{14}$ m^{-2}, based on H_2O/D_2O contrast exchange experiments. This corresponds to H_2O/Si in the range of 1.8–1.4, and a scattering contrast between C-S-H and H_2O in the range of $(9.7-12.0) \times 10^{28}$ m^{-4}. Further CH_3OH/CD_3OH SANS contrast experiments and comparisons between SANS and SAXS [23] suggest a contrast value (between C-S-H and H_2O) of 10.7×10^{28} m^{-4}, which is used in the present study. The uncertainty in the contrast value for normal cement paste results in systematic uncertainties in the SANS surface area values of about $\pm 10\%$, but does not affect relative comparisons between different leached samples.

3. Experimental

Decalcification experiments were performed using pastes made from both WPC (US Gypsum) [24] and C_3S. The mineral composition by mass of the WPC is 72% C_3S, 17% C_2S, 5% C_3A, 1% C_4AF, and 0.7% alkalis. Pure triclinic C_3S was made by repeatedly calcining a 3:1 mixture by mass of CaO and SiO_2 powder at 1430 °C and then grinding the resulting product in a mortar and pestle. X-ray analysis indicated no unreacted CaO. The WPC and C_3S powders were mixed at a water-to-cement ratio (w/c) of 0.5 by mass and allowed to hydrate under saturated conditions. Specimens were tested at the age of either 6 or 3.5 months, as noted below. SANS specimens were prepared a few days before the experiment by cutting the pastes into 0.8-mm-thick coupons using a water-lubricated wafering saw. Decalcification was then performed by placing the coupons into a 6-mol/l aqueous solution of NH_4NO_3. The mass loss of the specimens was monitored by periodically removing and

weighing them as they leached, and samples were removed and rinsed with deionized water when they reached a preselected mass loss value. Because leaching is a diffusion-controlled process, composition gradients inevitably develop across the sample thickness, and thus there is overlap between the removal of CH and the decalcification of C-S-H. Quantitative X-ray diffraction was used to measure the CH content in a parallel series of leached specimens with the same geometry, and the CH was found to be completely removed when the bulk C/S reached 1.4 [10].

To determine accurately the calcium and silicon contents of the pastes (i.e., the C/S), approximately 0.1 g of specimen was interground with LiB_4 flux and heated to 1000 °C in a graphite crucible, vitrifying the sample. The glassy sample could then be completely dissolved in dilute HCl. The elemental Ca and Si concentrations of the resulting aqueous solutions were measured using ICP-AES with appropriate standard reference solutions. Tests conducted using a standard OPC showed that this procedure was accurate to within 1%. The bound water contents of the pastes were calculated by first vacuum drying a specimen of coarsely ground paste over water at the temperature of dry ice (D-drying) and then measuring the mass loss after ignition at 1000 °C.

Two separate SANS experiments were performed using the 30-m SANS instruments [25] at the National Center for Neutron Research in Gaithersburg, MD. During the first experiment, 6-month-old C_3S and WPC pastes, including all of the contrast variation experiments, were conducted using the NG3 SANS instrument. During the second experiment, 3.5-month-old WPC pastes were measured using the similar NG7 SANS instrument. All SANS measurements were performed on coupons of saturated paste using a neutron wavelength of 0.8 nm. For the WPC paste specimens, three sample-to-detector distances were used, giving an effective Q range of 0.03–2.2 nm^{-1}. The C_3S pastes were measured only at the shortest distance, so that the lower limit in Q for this case was about 0.3 nm^{-1}.

Contrast variation experiments were performed using five coupons of paste at each C/S. The coupons were first analyzed with SANS while saturated with H_2O to establish the initial C_P. Then, the coupons were placed in H_2O/D_2O mixtures with D_2O mole fractions of 0.2, 0.4, 0.6, 0.8, and 1.0 and allowed to exchange for a period of 24–36 h. They were then analyzed again to determine the new C_P, taking care to measure the same location on the coupon so as to minimize the possible effects of any microstructure spatial variation. The contrast variation as a function of D_2O content was expressed as the ratio of the second C_P to the first C_P for each coupon.

Surface areas were measured using an automated nitrogen gas sorption unit (Omnisorp 360, Coulter, Hialeah, FL), and the data were analyzed using the multipoint BET method [26]. Specimens were prepared for gas sorption by D-drying for a period of at least 10 days.

4. Results

4.1. SANS response of leached paste

The scattering data for the unleached WPC paste and the WPC pastes leached to C/S of 2.5 and 1.54 are shown in Fig. 2. The overall intensity of the scattering remains fairly constant, but there are changes in the shape of the curves. There is a slight loss of intensity at low Q values, caused by the dissolution of small (<1 μm) CH crystals, and possibly some loss in the C-S-H surface fractal component, while at higher Q, there is a change in the slope of the volume fractal regime, particularly for the C/S = 1.54 specimen. Fig. 3 shows the scattering response for WPC pastes leached to C/S < 1.0. At C/S = 0.83, there is a significant increase in the scattered intensity in both the volume fractal and Porod regions as compared to the unleached paste. On further leaching to C/S = 0.68, there is significant increase in the scattered intensity across the entire Q range. While the crossover between the volume fractal and surface fractal regimes remains in roughly the same place (0.2–0.3 nm^{-1}), the upper cutoff in Q for the volume fractal regime moves to the left and the fractal exponent changes, suggesting a coarsening and change in morphology of the fine structure of the leached C-S-H gel. Finally, at C/S = 0.33, the Porod region shifts significantly to the left and the Porod intensity is decreased, indicating either an increase in the size of the fundamental gel particles or a thickening of the sheet structures (discussed below) that result from leaching.
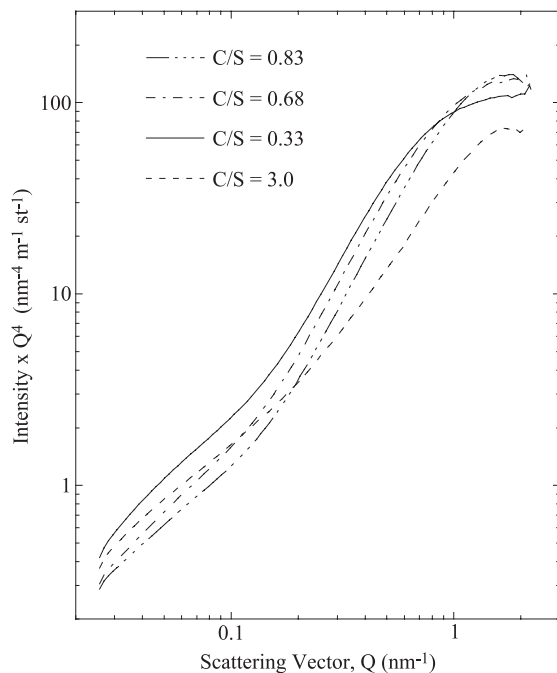

Fig. 3. SANS response of 6-month-old WPC pastes leached to C/S below 1.0. The unleached paste is also shown for comparison. The large increase in scattering intensity at higher Q with leaching can be attributed to increased access to the C-S-H gel phase.

C_3S pastes leached to C/S = 1.7 and C/S = 0.8 exhibited behavior similar to that of leached WPC paste.

Table 1 lists the apparent power law exponents and the range of Q over which volume fractal behavior is observed in the WPC pastes. The apparent volume fractal slopes are generally less steep than those previously derived from a multicomponent model [13] because that model accounts for the superimposition of the volume fractal and surface fractal components over much of the Q range measured. However, the breakdown of such models as leaching progresses (at least regarding the volume fractal component) justifies the more empirical observations presented here. Decalcification causes the exponent, x, to change from an initial apparent value of 2.38 to a minimum value of 1.84, and then to increase again to near 2.0. Scattering that follows a Q^{-2} power law is generally the hallmark of a sheet- or foil-like morphology [27] and thus the present results are in agreement with microscopic evidence that C-S-H gel formed with C/S near 1.0 has a foil-like morphology [11].

As C/S decreases, the upper and lower limits of the volume fractal regime both move to lower Q values (see Table 1). In cement systems, the observed lower limit of volume fractal scaling generally represents the point where the relative contribution from surface fractal scattering becomes important. The observed slight decrease in the lower Q limit for the power law scattering therefore reflects an increasing dominance of the volume fractal component of the microstructure over the surface fractal component as leaching progresses. Deviation from Q^{-x} scattering at the high end of the volume fractal range occurs when the scattering form–factor for the structural building blocks of the volume fractal regime becomes the dominant contribution to the scattered intensity. The Q value where this occurs is inversely proportional to the size of the building blocks. Thus, the decrease in the upper limit of the volume fractal regime with leaching suggests that either the C-S-H gel globules increase in size with leaching, or that the sheets formed on leaching become thicker as leaching progresses. The shift in the curves to lower Q values shown in Fig. 3 indicates that for C/S = 0.33, the sheets have thickened to roughly a double layer of the original 5 nm gel globules.

The data shown in Figs. 2 and 3 indicate that as the C/S decreases, roughly equiaxed 5 nm C-S-H particles transform into larger sheetlike structures. This is in good agreement with the known increase in the average linear silicate chain length with decreasing C/S, and with the well-established (e.g., Ref. [28]) similarity of C-S-H phases with C/S near 1 to the layered mineral tobermorite (C/S = 0.83). The significantly higher C/S of C-S-H gel in normal cement pastes causes the structure to become highly disordered, so that no layered structure exists on length scales greater than a few nanometers. As calcium is removed from this structure, the silicates can rearrange into longer chains and this allows for an increase in long-range order. ^{29}Si NMR analysis of leached C_3S pastes (reported in detail elsewhere, [7]) shows that the average chain length begins to increase rapidly with

Table 1
Power law fits to the volume fractal region of the SANS data for leached WPC pastes

Paste	C/S ratio	Power x in Q^{-x} [a]	Range of Q (nm^{-1})
WPC, 6 months old	3.0	2.381(6)	0.3–0.8
	2.4	2.283(7)	0.3–0.8
	1.56	2.097(7)	0.3–0.8
	0.83	1.836(4)	0.25–0.7
	0.68	1.906(3)	0.2–0.7
	0.33	1.946(4)	0.2–0.5
WPC, 3.5 months old	3.0	2.430(6)	0.3–0.8
	1.47	2.014(5)	0.3–0.8
	1.14	1.848(5)	0.3–0.7
	0.91	1.907(4)	0.25–0.7
	0.50	2.094(4)	0.25–0.5

[a] The number in parentheses is the uncertainty for the last digit computed from the power law fit.

decalcification at C/S < 1.2, and that at C/S near 0.3, there are significant amounts of Q_3 and Q_4 groups (where Q_n indicates a silicate bonded to n other silicates) indicating a shift toward a silica gel structure. The degree of polymerization of the silicates as measured by ^{29}Si NMR has also been shown to be greater in lower C/S pastes made with silica-rich mineral admixtures [29,30].

Fig. 4 shows the Porod constant of the WPC and C_3S pastes as a function of leaching. The Porod constant increases as the C/S decreases, reaching a maximum value at approximately C/S = 1.0, and then decreases again with further decalcification. The WPC and C_3S pastes are in good agreement. This strongly suggests that the measured surface area increases significantly on leaching (see Eq. (3)), al-
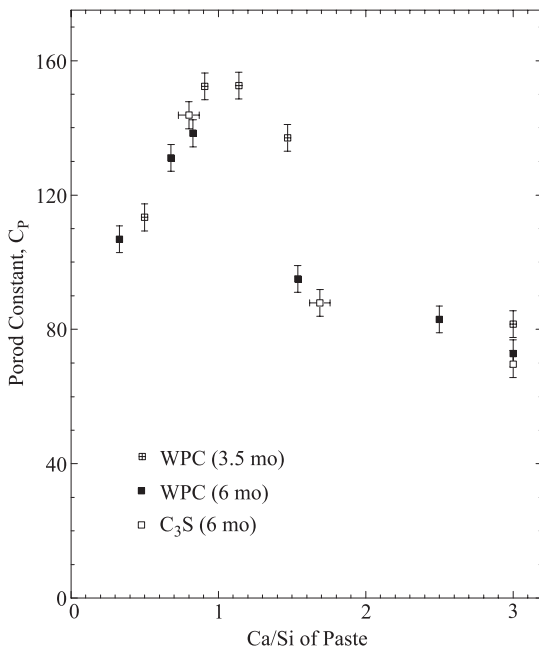
though it should be noted that an increase in the scattering contrast between C-S-H and the pore fluid could increase the observed SANS intensity and C_P value without any microstructural changes. As is shown in the following section, the contrast increases by only about 10% on decalcification to C/S = 1, so this does not account for the factor of two increase in C_P shown in Fig. 4. The effects of leaching on the surface area are discussed further in Sections 4.3 and 5.

4.2. H_2O/D_2O exchange experiments

Fig. 5 shows the SANS data for three of the WPC pastes before and after exchange of the pore fluid with pure D_2O. For the unleached WPC paste, D_2O exchange causes the SANS data to have a very different shape. At high Q, the large decrease in intensity reflects the decrease in the neutron scattering contrast when C-S-H exchanges to form C-S-D. With decreasing Q (representing scattering from larger features) the intensity of the scattering from the D_2O-exchanged paste increases significantly relative to, and eventually surpasses that of, the hydrated paste. Because H_2O/D_2O exchange does not affect the microstruc-
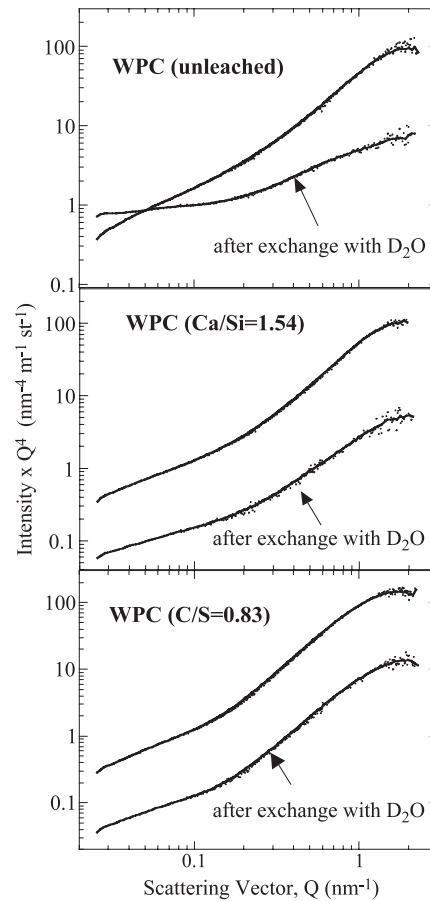

Fig. 4. Porod constant (determined from high-Q SANS data) as a function of the total C/S of the specimens. Vertical bars indicate computed standard deviations from the Porod fits.

Fig. 5. Effect of D_2O exchange on the SANS data. Top: normal WPC paste. Middle: WPC leached to C/S = 1.54. Bottom: WPC leached to C/S = 0.83. The change in the shape of the D_2O-exchanged data is caused by the removal of calcium hydroxide; see text.

ture, this can only be caused by an increase in scattering contrast caused by increased scattering intensity from coarser phases, such as CH, that do not exchange with the D_2O. When C-S-H exchanges to form C-S-D, the scattering contrast with the pore fluid decreases by a factor of more than 10, whereas the contrast between pore fluid and nonexchanging CH increases by a factor of 5. Fig. 5 also shows the same type of plot for the WPC pastes leached to C/S = 1.54 and C/S = 0.83. At C/S = 1.54, exchange with D_2O significantly decreases the SANS intensity at all Q values, and at C/S = 0.83, the D_2O-exchanged and -unexchanged scattering curves are parallel across the entire Q range sampled, indicating that microstructural features at all length scales exchanged fully with D_2O.

Fig. 6 shows the results of three of the contrast exchange experiments conducted on leached WPC pastes. The relative contrast, obtained by normalizing the C_P values obtained after D_2O exchange to the initial (pure H_2O) C_P values, is plotted against the mole fraction of D_2O in the exchange fluid. Similar curves were obtained for C_3S pastes. The data for each paste is parabolic, as expected. The shape of the curves verifies that the overwhelming majority of the H_2O present in the solid phases that generate the Porod scattering exchanged with the pore fluid. Lack of full exchange would result in contrast minimums to the left of those found and would give significantly more scattering intensity for the fully D_2O-exchanged coupons.

The results of the contrast variation experiments are listed in Table 2. For the C/S = 3.0 (unleached) and C/S = 2.5 samples, the minimum in the fitted parabola was slightly greater than zero, indicating a small scattering
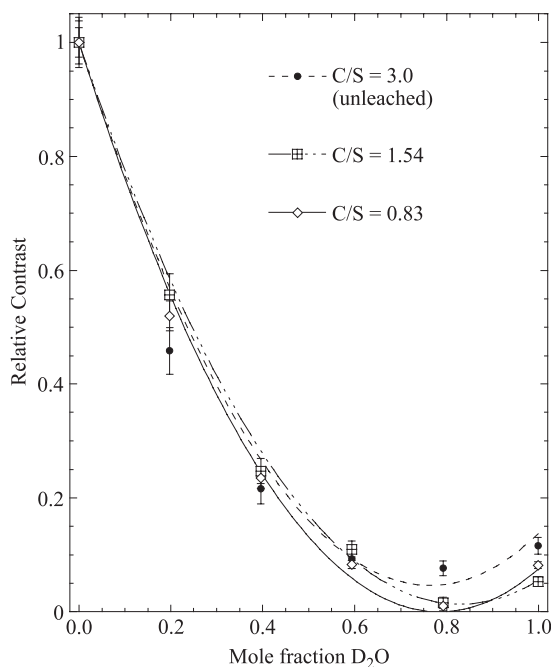
Table 2
Results of the contrast exchange experiments and estimated C-S-H/H_2O neutron scattering contrast values

Paste type	C/S ratio	Fit type	Fitted intensity from CH (%)	C-S-H matchpoint (%D_2O)	H_2O/Si ratio	C-S-H:H_2O contrast ($\times 10^{28}$ m^{-4})
WPC	3.0	2 parabolas	2.1	82.77	1.60	10.7
WPC	2.4	2 parabolas	1.0	79.57	1.60	10.7
WPC	1.56	1 parabola	0	82.33	1.47	11.1
WPC	0.83	1 parabola	0	78.45	0.93	12.3
WPC	0.68	1 parabola	0	79.16	0.81	13.0
WPC	0.33	1 parabola	0	72.71	0.53	13.6
C_3S	3.0	2 parabolas	0.8	77.82	1.60	10.7
C_3S	1.7	1 parabola	0	82.25	1.60	10.7
C_3S	0.8	1 parabola	0	79.04	0.89	12.7

contribution from fine crystalline CH that does not exchange with the pore fluid [23]. These curves were therefore fit as the sum of two parabolas with minimum values constrained to be zero: one representing CH with a minimum constrained to the known matchpoint value of 32% D_2O, and the other with a variable matchpoint representing the C-S-H gel. The resulting percentage of the Porod scattering intensity arising from CH is also listed in Table 2. The measured parabolas at lower C/S all have a minimum very close to zero (see Fig. 6), indicating that the SANS in the Porod regime arises from C-S-H alone. Each of the curves for low C/S was fitted using a single parabola with a minimum relative contrast value of zero, and these contrast variation results confirm the expected removal of CH during the initial stages of leaching.

Fig. 7 shows the C-S-H contrast matchpoint as a function of C/S ratio. The matchpoint remains at roughly 81% D_2O during initial leaching, in agreement with previous measurements of unleached pastes, and then moves slightly to the left (lower D_2O mole fractions) with leaching at C/S below 1.54. The behavior of the WPC and C_3S pastes is similar. The relatively small changes in the position of the contrast minimum with leaching indicate that there are correspondingly minor changes in the C-S-H/H_2O contrast. As indicated earlier, once the C/S and the C-S-H contrast matchpoint are known, the scattering length density of C-S-H can be determined if either the H_2O/Si or the density is known. As the density is difficult to measure due to the fine gel pore structure [31], the H_2O/Si ratio was evaluated by measuring the bound water content as a function of leaching. C_3S pastes were used to eliminate the effects of aluminate phases present in cements. As shown in Fig. 8, the H_2O/Si of the pastes decreases with decreasing C/S. This is consistent with other published data from synthetic C-S-H [32] and from the C-S-H gel present in blended cement pastes such as OPC with silica fume [30].

Fig. 8 shows that a significant amount of bound water remains in the C-S-H even at C/S as low as 0.2, indicating that the structure is still quite different from that of pure amorphous SiO_2. This is in agreement with the contrast matchpoint data plotted in Fig. 7: the calculated contrast

Fig. 6. Contrast variation with H_2O/D_2O exchange, for three of the WPC pastes. The lines are parabolic fits (as explained in the text) and vertical bars indicate computed standard uncertainties for each point.
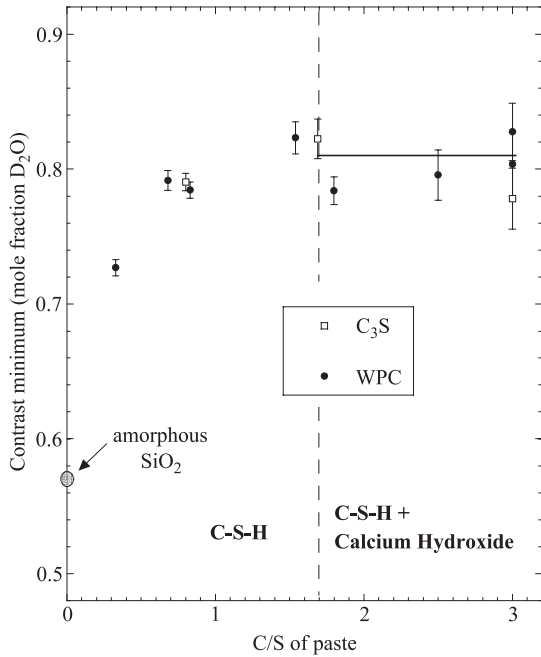
Fig. 7. Contrast minimum for scattering between C-S-H and the pore fluid, as a function of leaching. The horizontal line represents the previously determined average value for cement and C_3S pastes. Vertical bars indicate computed uncertainties.

matchpoint for pure silica gel (density = 2.2 g/cm^3) is at 57% D_2O, considerably less D_2O-rich than the matchpoint of 72% observed for the C/S = 0.33 specimen. For unleached C_3S paste, the H_2O/Si after D-drying is about 1.4, in agreement with published values [31]. This is slightly lower

than the H_2O/Si value of 1.6 assumed for the C-S-H/H_2O scattering contrast of unleached pastes in this study. It should be noted that the C-S-H composition after D-drying would not necessarily be expected to correspond to the solid C-S-H phase probed by neutrons, as D-drying may remove some tightly adsorbed water that behaves as part of the solid phase forming an interface with liquid water, and this may also collapse the structure.

To estimate the scattering contrast for C-S-H with C/S < 1.5, the linear fit to the bound water data shown in Fig. 8 was used to estimate the decrease in H_2O/Si on leaching. These H_2O/Si, and the resulting C-S-H/H_2O contrast values, are listed in Table 2. The contrast value increases slightly with leaching.

4.3. Surface area of leached pastes

Fig. 9 shows the surface area of the pastes as a function of C/S, calculated using Eq. (3) and the contrast values listed in Table 2. The surface area does in fact increase significantly with leaching, slightly more than doubling from the initial value to the observed maximum near C/S = 1.0.

To verify this trend, the surface area of 6-month-old WPC paste specimens were measured using nitrogen BET. When reported in the standard specific surface area units of m^2/g of specimen, the BET surface area increased dramatically with leaching. However, this resulted in large part from the significant decrease in sample weight with leaching, and is thus misleading. To convert the nitrogen BET values to the intrinsic SANS units of surface area per unit
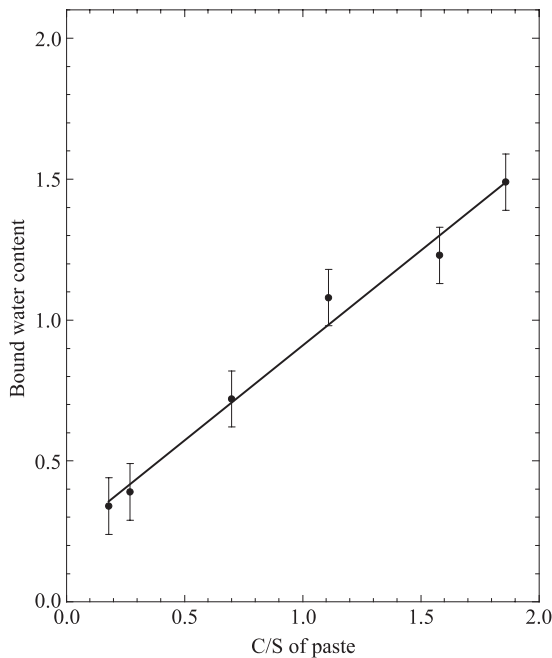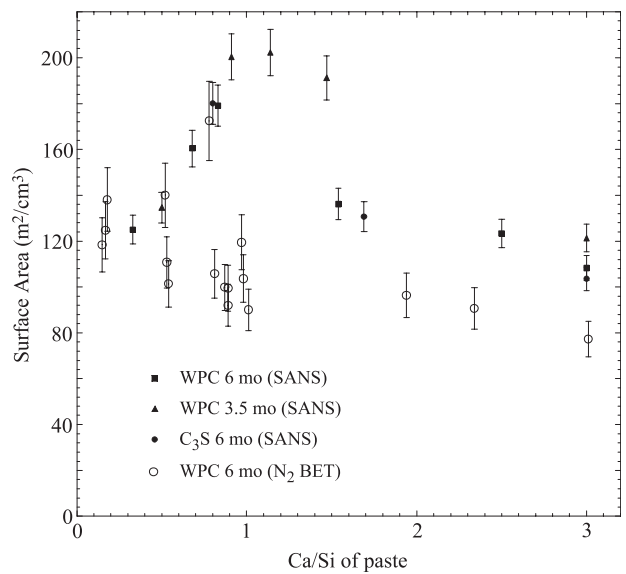

Fig. 8. The bound water content of WPC paste (molar H_2O/Si ratio) as a function of C/S ratio. The line is a linear fit to the data. Vertical bars indicate estimated uncertainties.

Fig. 9. Surface area (per unit specimen volume) as a function of leaching. Both SANS and N_2 BET results are plotted. The BET values were renormalized to a volume basis (see text). Vertical bars on the SANS data indicate computed uncertainties from the Porod fits, and vertical bars on the BET data indicate uncertainties estimated from repeat runs on selected specimens.

volume, the density of D-dried WPC pastes was also measured as a function of leaching. The resulting renormalized BET surface area values are also plotted in Fig. 9. The BET values increase with leaching, although not as sharply as the SANS values. The agreement between the SANS and BET values is reasonable, given the rather significant effects of drying on the C-S-H gel, although the BET data do not appear to show the significant increase in surface area between C/S = 1.5 and C/S = 1.0 seen with SANS.

5. Discussion

The amount of C-S-H in a paste, when expressed per mole of SiO_2, should not change on calcium leaching, and the size of the C-S-H particles, as determined from Guinier fits and fractal modeling of the SANS data, decreases only slightly on initial leaching and then increases. This suggests that the large increase in the measured surface area with decalcification (see Fig. 9) is caused not by an increase in the specific surface area of the C-S-H, but rather by an increase in the amount of C-S-H with a high specific surface area that is accessible to SANS and nitrogen sorption. The C-S-H gel in cement paste forms with two morphologies, commonly referred to as outer product and inner product, and there is evidence that under normal conditions, only the lower density form has a high surface area as measured by SANS [16] or by nitrogen BET [33]. An obvious explanation for the increase in surface area with decalcification is that the leaching process opens up the high-density C-S-H structure, giving it a high measurable surface area. This hypothesis is well supported by other evidence, as discussed below.

The SANS surface area values should be consistent with the overall microstructural picture generated by the SANS data at different scattering vectors. The latter shows cement paste to be a random fractal structure built up from 5 nm globules. For a solid phase consisting of noncontacting 5-nm-diameter spheres, the surface area per unit solid volume is 1200 m^2/cm^3. For a mature paste with w/c = 0.5 (as used here), the volume fraction of solid C-S-H (excluding porosity) is ≈ 0.3 (Ref. [31], p. 239); thus, the theoretical maximum surface area per unit sample volume prior to leaching (ignoring contributions from other phases) is about 360 m^2/cm^3. On allowing for surface contacts, volume fractal models [13] suggest a local packing fraction of around 60% by volume and, therefore, a reduction in the expected surface area (if all C-S-H is accessible) to around 200 m^2/cm^3—significantly higher than the measured SANS surface area of unleached paste but close to the maximum value for leached paste.

Tennis and Jennings [33] have demonstrated that variability in nitrogen gas sorption measurements of surface area and pore volume can best be modeled by assuming that only the low-density form of C-S-H has a surface area measurable by nitrogen sorption. This model predicts that about 65 vol.% of the C-S-H in a well-hydrated paste with w/c = 0.5 is of the low-density type. If one assumes that only 65% of the C-S-H gel in the unleached pastes has a high surface area, the estimated surface area per unit sample volume for the accessible C-S-H decreases from about 200 m^2/cm^3 to about 130 m^2/cm^3, reasonably close to the measured value.

Based on published SANS, gas sorption, and density data for cement paste, Jennings [20] has proposed that the low- and high-density forms of C-S-H are both formed from the same 5 nm C-S-H globules, but with different characteristic packing densities. Recent nanoindentation experiments [34–36] have provided striking support for this structural model of C-S-H gel. Statistical analysis of multiple nano-indents show that the C-S-H phase has two characteristic stiffness values at the nanometer scale that can be associated with high- and low-density C-S-H. For a normal OPC paste with a w/c of 0.5, Constantinides and Ulm [35] reported stiffness values of 21.7 and 29.4 GPa and associated volume fractions of 70% and 30%. These volume fractions are in good agreement with the model predictions noted above. Acker [34] reported very similar characteristic stiffness values (20 and 31 GPa) for a high-performance cement with w/c = 0.3, indicating that the morphology of the two C-S-H types is to some extent independent of the processing and curing conditions. Ulm et al. [36] then showed that if the two C-S-H types with different stiffnesses are assumed to consist of the same solid phase with different characteristic porosities, then the porosity values must be the same as the values predicted by the Jennings [20] structural model.

Constantinides and Ulm [35] also performed nanoindentation on a cement paste after decalcification to C/S = 1, and found that the volume fractions of the two C-S-H types were unchanged, while the characteristic stiffness values decreased significantly. They attributed the stiffness decrease primarily to an increase in the intrinsic porosity of the high- and low-density C-S-H.

All of the above evidence indicates that the high-density C-S-H contributes to the surface area measured by SANS and by nitrogen BET only after it is decalcified. It should be noted that the low-density C-S-H is also strongly affected by leaching, and its contribution to the surface area could increase somewhat as well during initial decalcification when the overall surface area is increasing. Continued leaching below C/S = 1 appears to cause a thickening of the (now sheetlike) fundamental C-S-H units and a consequent decrease in the measured surface area.

6. Summary

Decalcification of cement and tricalcium silicate (C_3S) pastes by leaching increased the SANS intensity across the entire volume fractal regime corresponding to C-S-H gel, and the surface area per unit specimen volume, determined from the SANS intensity at the highest scattering vectors, nearly doubled on decalcifying the C-S-H from C/S = 1.7 to C/

S = 1.0. The surface area per unit volume measured by nitrogen gas sorption on dried specimens increased more gradually with decalcification and did not show a sharp maximum near C/S = 1. The best explanation for these results is that the high-density "inner-product" C-S-H gel, which normally has a low specific surface area as measured by SANS and nitrogen gas sorption, is transformed by the leaching process into a morphology with a high specific surface area. This explanation is supported by recent nanoindentation results indicating that the internal porosity of the high-density form of C-S-H gel is increased by calcium leaching.

Decalcification also changed the apparent volume fractal scaling exponent of the SANS data from 2.3 to about 2.0. This indicates that the equiaxed 5 nm C-S-H globule building blocks (first identified in previous SANS work) that form the volume fractal microstructure of normal, unleached cement paste are transformed by decalcification into sheetlike structures of increasing thickness. This in agreement with the well-established link between low-C/S C-S-H phases and the layered mineral tobermorite.

Acknowledgements

References

[1] M. Mainguy, O. Coussy, Propagation fronts during calcium leaching and chloride penetration, J. Eng. Mech., vol. 126, ASCE, 2000, pp. 250–257.

[2] M. Mainguy, F.J. Ulm, F.H. Heukamp, Similarity properties of demineralization and degradation of cracked porous materials, Int. J. Solids Struct. 38 (2001) 7079–7100.

[3] C. Carde, R. Francois, J.M. Torrenti, Leaching of both calcium hydroxide and C-S-H from cement paste: Modeling the mechanical behavior, Cem. Concr. Res. 26 (1996) 1257–1268.

[4] F.-J. Ulm, J.M. Torrenti, F. Adenot, Chemoporoplasticity of calcium leaching in concrete, J. Eng. Mech., vol. 125, ASCE, 1999, pp. 1200–1211.

[5] F.H. Heukamp, F.-J. Ulm, J.T. Germaine, Mechanical properties of calcium-leached cement pastes: triaxial stress states and the influence of the pore pressures, Cem. Concr. Res. 31 (2001) 767–774.

[6] F.H. Heukamp, F.-J. Ulm, J.T. Germaine, Poroplastic properties of calcium-leached cement-based materials, Cem. Concr. Res. 33 (2003) 1155–1173.

[7] J.J. Chen, J.J. Thomas, H.F.W. Taylor, H.M. Jennings, Solubility and structure of calcium silicate hydrate, Cem. Concr. Res. 34 (2004) 1499–1519.

[8] P. Yu, R.J. Kirkpatrick, B. Poe, P.F. McMillan, X. Cong, Structure of calcium silicate hydrate (C-S-H): near-, mid-, and far-infrared spectroscopy, J. Am. Ceram. Soc. 82 (1999) 742–748.

[9] K. Haga, M. Shibata, M. Hironaga, S. Tanaka, S. Nagasaki, Silicate anion structural change in calcium silicate hydrate gel on dissolution of hydrated cement, J. Nucl. Sci. Technol. 39 (2002) 540–547.

[10] J.J. Thomas, D.A. Neumann, J.J. Chen, H.M. Jennings, Ca-OH bonding in decalcified portland cement and tricalcium silicate pastes measured by inelastic neutron scattering, Chem. Mater. 15 (2003) 3813–3817.

[11] I.G. Richardson, G.W. Groves, Microstructure and microanalysis of hardened cement pastes involving ground granulated blast-furnace slag, J. Mater. Sci. 27 (1992) 6204–6212.

[12] C. Carde, G. Escadeillas, R. Francois, Use of ammonium nitrate solution to simulate and accelerate the leaching of cement pastes due to deionized water, Mag. Concr. Res. 49 (1997) 295–301.

[13] A.J. Allen, R.C. Oberthur, D. Pearson, P. Schofield, C.R. Wilding, Development of the fine porosity and gel structure of hydrating cement systems, Philos. Mag., B 56 (1987) 263–268.

[14] D.N. Winslow, S. Diamond, Specific surface of hardened cement paste as determined by small-angle X-ray scattering, J. Am. Ceram. Soc. 57 (1974) 193–197.

[15] R.E. Beddoe, K. Lang, Effect of moisture on fractal dimension and specific surface of hardened cement paste by small-angle X-ray scattering, Cem. Concr. Res. 24 (1994) 605–612.

[16] J.J. Thomas, H.M. Jennings, A.J. Allen, The surface area of cement paste as measured by neutron scattering—Evidence for two C-S-H morphologies, Cem. Concr. Res. 28 (1998) 897–905.

[17] A.J. Allen, R.A. Livingston, Relationship between differences in silica fume additives and fine-scale microstructural evolution in cement based materials, Adv. Cem. Based Mater. 8 (1998) 118–131.

[18] J.J. Thomas, H.M. Jennings, A.J. Allen, The surface area of hardened cement paste as measured by various techniques, Concr. Sci. Eng. 1 (1999) 45–64.

[19] J.J. Thomas, D.A. Neumann, S.A. FitzGerald, R.A. Livingston, State of water in hydrating tricalcium silicate and portland cement pastes as measured by quasi-elastic neutron scattering, J. Am. Ceram. Soc. 84 (2001) 1811–1816.

[20] H.M. Jennings, A model for the microstructure of calcium silicate hydrate in cement paste, Cem. Concr. Res. 30 (2000) 101–116.

[21] V.F. Sears, Neutron scattering lengths and cross-sections of the elements and their isotopes (special feature), Neutron News 3.3 (1992) 29–37.

[22] J.J. Thomas, H.M. Jennings, A.J. Allen, Determination of the neutron scattering contrast of hydrated portland cement paste using H_2O/D_2O exchange, Adv. Cem. Based Mater. 7 (1998) 119–122.

[23] A.J. Allen, J.J. Thomas, H.M. Jennings, Composition and density of amorphous calcium silicate hydrate gel in cement systems from combined neutron and X-ray small angle scattering (in preparation).

[24] Information on commercial products is given for completeness and does not constitute or imply their endorsement by the National Institute of Standards and Technology.

[25] C.J. Glinka, J.G. Barker, B. Hammouda, S. Kreuger, J.J. Moyer, W.J. Orts, The 30 m small-angle neutron scattering instruments at the National Institute of Standards and Technology, J. Appl. Crystallogr. 31 (1998) 430–445.

[26] S. Brunauer, P.H. Emmit, E. Teller, Adsorption of gases in multimolecular layers, J. Am. Chem. Soc. 60 (1938) 309–319.

[27] G. Porod, in: O. Glatter, O. Kratky (Eds.), Small-Angle X-ray Scattering, Academic Press, London, 1982, pp. 17–51.

[28] X. Cong, R.J. Kirkpatrick, ^{29}Si MAS NMR study of the structure of calcium silicate hydrate, Adv. Cem. Based Mater. 3 (1996) 144–156.

[29] Z.-Q. Wu, J.F. Young, The hydration of tricalcium silicate in the presence of colloidal silica, J. Mater. Sci. 19 (1984) 3477–3486.

[30] P. Lu, G. Sun, J.F. Young, Phase composition of hydrated DSP cement pastes, J. Am. Ceram. Soc. 76 (1993) 1003–1007.

[31] H.F.W. Taylor, Cement Chemistry, 2nd ed., Thomas Telford, London, 1997.

[32] X. Cong, R.J. Kirkpatrick, ^{29}Si MAS NMR study of the structure of calcium silicate hydrate, Adv. Cem. Based Mater. 3 (1996) 144–156.

[33] P.D. Tennis, H.M. Jennings, A model for two types of calcium silicate hydrate in the microstructure of portland cement pastes, Cem. Concr. Res. 30 (2000) 855–863.

[34] P. Acker, in: F.J. Ulm, Z.P. Bazant, F.H. Wittmann (Eds.), Creep, Shrinkage, and Durability Mechanics of Concrete and other Quasi-Brittle Materials, Elsevier, New York, 2001, pp. 15–25.

[35] G. Constantinides, F.-J. Ulm, The effect of two types of C-S-H on the elasticity of cement-based materials: Results from nanoindentation and micromechanical modeling, Cem. Concr. Res. 34 (2004) 67–80.

[36] F.-J. Ulm, G. Constantinides, F.H. Heukamp, Is concrete a poromechanics material? A multiscale investigation of poroelastic properties, Mater. Struct. 37 (2004 (Jan–Feb)) 43–58.